A Purely Spaceborne Open Source Approach for Regional Bathymetry Mapping

Nathan Thomas, Brian Lee, Oliver Coutts, Pete Bunting, David Lagomasino, and Lola Fatoyinbo

***Abstract*— Timely and up-to-date bathymetry maps over large geographical areas have been difficult to create, due to the cost and difficulty of collecting *in situ* calibration and validation data. Recently, combinations of spaceborne Ice, Cloud, and Elevation Satellite-2 (ICESat-2) lidar data and Landsat/sentinel-2 data have reduced these obstacles. However, to date, there have been no means of automatically extracting bathymetry photons from ICESat-2 tracks for model calibration/validation and no well-established open source workflows for generating regional scale bathymetric models. Here we provide an open source approach for generating bathymetry maps for the shallow water region around the island of Andros, Bahamas. We demonstrate an efficient means of processing 224 ICESat-2 tracks and 221 Landsat-8 scenes, using the classification of subaquatic height extracted photons (C-SHELPh) algorithm and Extra Trees Regression to provide 30 m pixel estimates of per-pixel depth and standard error. We map bathymetry with an RMSE of 0.32 m and RMSE% of 6.7%. Our workflow and results demonstrate a means of achieving accurate regional–scale bathymetry maps from purely spaceborne data.**

***Index Terms*— Bathymetry, Ice, Cloud and Elevation Satellite-2 (ICESat-2), landsat8, machine learning.**

I. Introduction

MAPS of shallow water bathymetry are critical for the provision of coastal socioecological services and emerging demands on the blue economy will open up new opportunities for development where up-to-date water depth information is needed. Marine navigation, aquaculture, climate change adaption and mitigation, coastal resilience, and disaster recovery are several key markets that will demand resources from the nearshore environment over the coming century [1]. Contemporary nearshore seafloor maps with regular repeat observations will enable proper marine spatial planning (MSP) and enable the sharing of coastal waters [2], [3]. This is particularly pertinent for Big Ocean States that have limited data access [4] and an inability to conduct expansive marine surveys. In addition, nearshore structure is increasingly sought as a nature-based risk reduction solution, predominantly focusing upon the use of natural barriers to sea level rise and storm surges [5]. Measuring the wave attenuation of benthic habitats, such as seagrasses and coral reefs [6] are aided with accurate maps of the seafloor, but this requires up-to-date and repeatable observations of sediment stability and structural complexity [7], [8]. These and other processes are not fully captured by current, openly available bathymetry data [9], which are limited in spatial and temporal resolution. There are several free and open initiatives that procure bathymetric data (e.g., International Hydrographic Organization Data Center for Digital Bathymetry (IHO DCDB; [10]), European marine observation and data network (EMODnet; [11]) and the general bathymetric chart of the oceans (GEBCO; [12]), but these are inadequate in shallow waters where the demands on vertical and spatial resolution are not met. High-resolution data can be derived from Singlebeam (SBES) and multibeam echo sounders (MBES) [13] but collecting data in shallow water is hazardous and time-consuming while bathymetric lidar data acquired from airborne systems [14] are economically expensive and time-intensive to collect.

Recent advances in satellite-derived bathymetry (SDB) using multispectral and hyperspectral Earth Observation have lead to new approaches and subsequent improved estimations [15], [16]. SDB studies have established the water depth retrieval through correlations between surface reflectance and field-acquired depth estimates [15], [17]–[26], but studies have so far been limited to single-site locations or processed small quantities of optical data. Methods that have used cloud computing have access to large archives of data [25] but often rely on data compositing, which reduces data volumes for bathymetry modeling and limits the derivation of per-pixel uncertainty.

Recently, spaceborne Ice, Cloud, and Elevation Satellite-2 (ICESat-2) data has emerged as a means of collecting bathymetry training data, enabling timely and consistent collections. Limited studies have begun to investigate bathymetric data calibration [27], [28] and a number of studies have generated study site to island scale maps of bathymetry at 10–30 m spatial resolution [25], [29]–[31]. These have predominantly relied on established linear relationships between optical reflectance and depth [17], [18], which recent tests have suggested can outperform machine learning approaches in

Manuscript received 15 April 2022; revised 20 June 2022; accepted 18 July 2022. Date of publication 21 July 2022; date of current version 4 August 2022. This work was supported by the NASA ICESat-2 Program under Grant NNH19ZDA001N-ICESAT2. *(Corresponding author: Nathan Thomas.)*

Nathan Thomas is with the Department of Biospheric Sciences, NASA Goddard Space Flight Center, Greenbelt, MD 20706 USA, and also with the Earth System Sciences Interdisciplinary Center, University of Maryland, College Park, MD 20740 USA (e-mail: nathan.m.thomas@nasa.gov).

Brian Lee is with the Bren School of Environmental Science, University of California, Santa Barbara, CA 93117 USA.

Oliver Coutts and Pete Bunting are with the Department of Geography and Earth Sciences, Aberystwyth University, Wales SY23 3DB, U.K.

David Lagomasino is with the Institute of Coastal Studies, East Carolina University, Wanchese, NC 27981 USA.

Lola Fatoyinbo is with the Department of Biospheric Sciences, NASA Goddard Space Flight Center, Greenbelt, MD 20706 USA.

Digital Object Identifier 10.1109/TGRS.2022.3192825

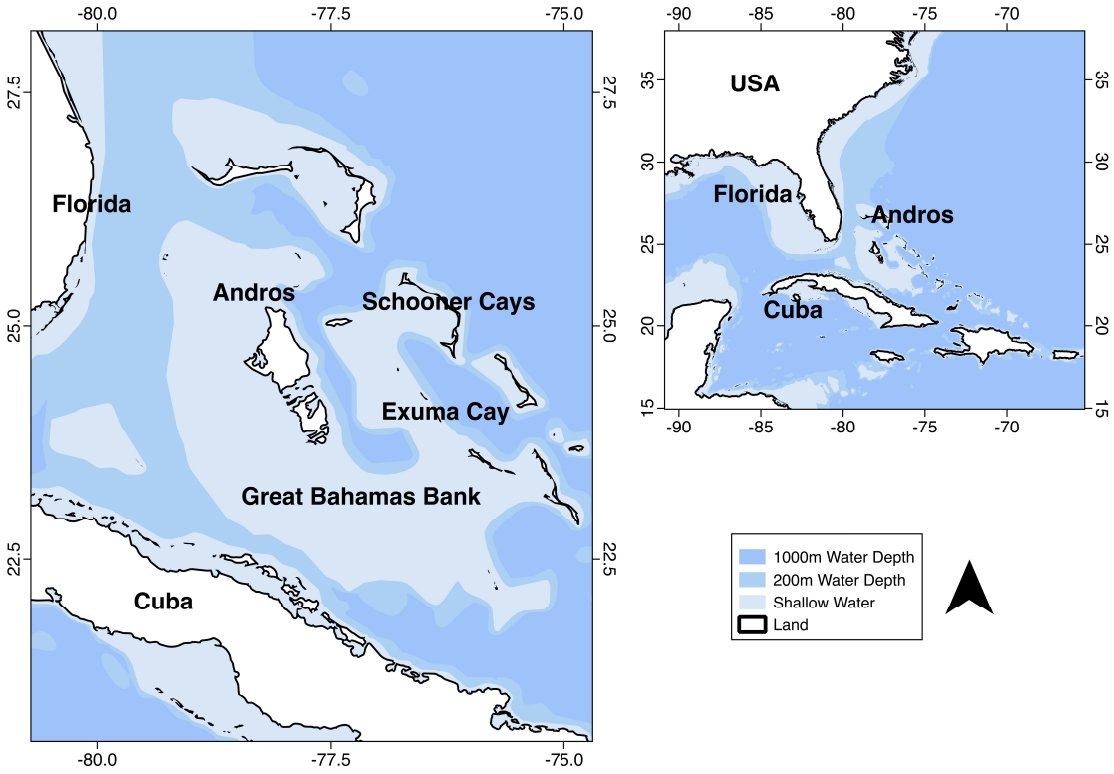

Fig. 1. Great Bahamas Bank study site, centered around the island of Andros in the Caribbean. Low-resolution bathymetry information and vector layers provided by Natural Earth. Free vector and raster map data available at www.naturalearthdata.com.

limited cases [25]. However, these tests were nonexhaustive and the role of machine learning has yet to be fully explored, particularly as they implement in—model weighting of variables based on the strength of the relationship which is not readily achieved with a linear or multilinear model. Despite this emergence, there are few available frameworks [32], [33] for ICESat-2 bathymetry photon extraction that are not labor and time intensive. Though commercial tools do exist for machine learning bathymetry extraction [34] there are currently no open–source tools capable of both extracting ICESat-2 bathymetric photons and generating robust bathymetry models. TCarta do provide both workflows and tools to achieve this but as a private commercial entity require substantial economic investment. Advances in this domain will help pave the way for a purely spaceborne SDB approach to mapping bathymetry at regional and larger scales [35], [36]. Here, we provide one such approach to alleviate these limitations, providing automated bathymetry photon extraction with a machine learning data fusion approach for modeling bathymetry with low error.

II. Methods

A. Study Site

The chosen study site is the Great Bahamas Bank around the island of Andros in the Bahamas, Caribbean (Fig. 1). Andros is a flat-topped isolated carbonate island bordered on the east by the tongue of the Ocean, a deep water region reaching a depth of 2000 m. Water depths within the Bahamas region are typically shallow (0–10 m) and contrast heavily with the Tongue of the Ocean and other surrounding deeper waters. Islands in the wider region are composed of Aeolian sands and limestone built on the Florida-Bahamas Platform. The wider Bahamas region is composed of 700 islands, cays and coral reefs and contains a number of distinct geomorphic features, including the Great Bahamas Bank. The region has a tropical climate which is heavily influenced by the Gulf Stream and hurricanes which frequently impact the region.

B. ICESat-2 Data

The ICESat-2 is a laser altimeter launched in September 2018. ICESat-2 carries a photon counting lidar, the advanced topographic laser altimeter system (ATLAS), which is composed of three pairs of beams each separated in the across-track direction by 3.3 km and 90 m between each pair. Each pair of lasers is divided into a strong and a weak beam, based on a 1:4 energy ratio. Each laser has a 10 KHz repetition rate at a wavelength of 532 nm. Each footprint has a diameter of 10 m and is separated by 70 cm. ICESat-2 geolocated photon data is provided in the ATL03 product [37]. Detailed instrument specifics can be found in [38]. All ICESat-2 data available over the study site were queried, subset, and downloaded from the National Snow and Ice Data Center (NSIDC) using the ICEPYX python software [39]. A total of 265 ICESat-2 tracks (version 5) were downloaded between 2021-01-03 through 2021-09-29, each containing up to three strong lasers each.

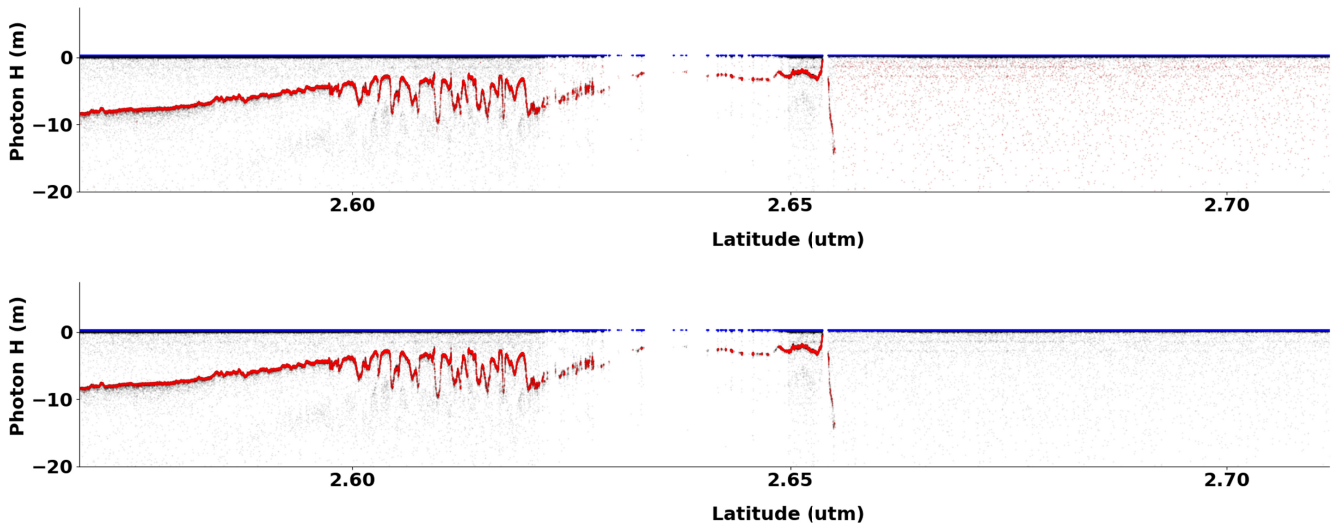

Fig. 2. Example of the manual selection of the C-SHELPh processed ICESat-2 tracks. Top: Poor isolation of the bathymetry surface with noise classified as surface points due to their density. This is evidenced by the red haze of classified photons near the blue water surface. Bottom: Successful identification of the bathymetric surface without the erroneous classification of noise photons (black). The quality of the signal-to-noise isolation determines the processed ICESat-2 photons selected for training.

To extract bathymetric photons from ICESat-2 tracks, we created the classification of subaquatic height extracted photons (C-SHELPh) python tool to locate and separate training photons. This algorithm detects the dense clustering of photons, synonymous with returns from a surface, over a dense grid whose dimensions are specified by user inputs. Default values include 0.5 m in the vertical (height) direction and 10 m in the horizontal (along-track latitude) direction. Photons are corrected for refraction following [27] and transformed to EGM08 from WGS84 ellipsoid height. Ocean surface temperature used for the refraction correction is retrieved automatically to match the ICESat-2 acquisition date and location from the Jet Propulsion Laboratory's GHRSST Level 4 Global Foundation Sea Surface Temperature Analysis via the OpenDap website [40]. Initially, dense clusters of photons detected around a height of 0 m are classified as ocean surface photons and the median height is used to determine a water surface. Below this value, dense photon clusters are identified on a per–grid–cell basis when meeting a user-defined threshold percentile value. This threshold value enables grids that include less dense noise photons where there are no bathymetric returns to be excluded. Once selected, the photon depth was determined from the water surface height and were output into a GeoPackage (GPKG) file. Only strong lasers were considered for this work. A suite of threshold values were run for each track and the best results were chosen based on manual inspection of the output plots. Manual inspection was determined based on both the quantity of incorrectly classified noise and accurately classified bathymetry surface photons (Fig. 2). This step ensures that no erroneous classified photons are used as training data and such is the ability of C-SHELph to classify millions of photons, even a conservative approach is able to yield large training data banks for modeling. In locations where high-resolution bathymetry data is available, this step could be automated by assessing the error of the ICESat-2 derived height in comparison to reference data. This generated 224 individual ICESat-2 bathymetric tracks to use as model training data.

All points within each GPKG that intersected a land mask polygon were removed to ensure no false training was provided. This provided a database of 18 954 960 bathymetric photons for model training. To reduce the compute time of the regression modeling a 5% subsample was extracted by selecting every 20th photon. The data was combined to create a training dataset of 947 748 photons, while the remainder was used for validation.

C. Landsat Imagery

Landsat 8 data was downloaded from the Google Public dataset (https://cloud.google.com/storage/docs/public-datasets/Landsat) using the tools within the atmospheric and radiometric calibration of satellite imagery (ARCSI) software [41]. For this study, all the Landsat 8 scenes from 2021 for 12 rows and paths of data that crossed the study site, with a cloud cover of 50% or less, were downloaded, totaling 221 scenes. Each of the Landsat images were then corrected to surface reflectance using a dark-subtraction algorithm within ARCSI and the United States Geological Survey (USGS) FMASK-provided cloud mask was applied to the imagery. A Shuttle Radar Topography Mission (SRTM) Digital Elevation Model (DEM) was used as input for the calibration. Each Landsat scene was corrected to 30 m spatial resolution in the local utm zone and included the blue, green, red, near-infrared (nir), shortware infrared (swir) and swir2 bands. After visual inspection, the FMASK was judged to perform poorly over water, thus an additional cloud mask was created. Pixels that intersected an independent water mask and had swir and swir2 bands >0.005 reflectance were classified as cloud. These pixels were then dilated using a 9×9 window. These new cloud masks were then applied

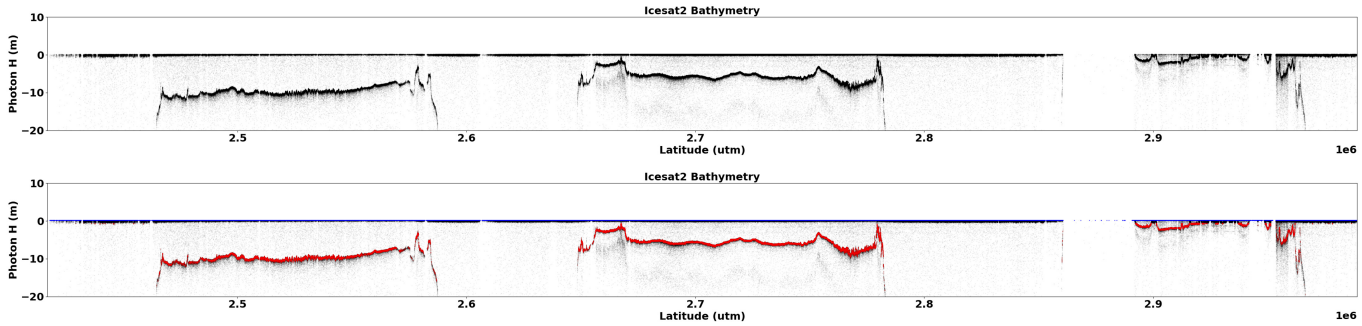

Fig. 3. ICESat-2 subaquatic photons. Top) Raw ICESat-2 data transformed to orthometric (EGM08) height. Bottom) Bathymetric classified photons (red) and surface classified photons (blue) from C-SHELPh. The algorithm is robust against a phenomenon known as ringing, whereby an artificial repeat of the surface is produced offset from the true surface, as visible below the red selected photons.

to the Landsat scenes to mask out remaining clouds. Finally, a land mask was used to remove all land surface pixels, leaving ocean pixels only.

D. Machine Learning Model

Additional preprocessing and data management was carried out using the Remote sensing and GIS Library (RSGISLib; [42]) python software. For each of the 221 Landsat scenes, the Landsat data was subset to the red, green, and blue bands and additional ratio bands of green/blue and blue/green were calculated to create a five-band image. For each bathymetric photon, the pixel value was extracted from each of the five image bands. These bathymetric depths and reflectance values were passed into a scikit-learn [43] Extra Trees Regressor via RSGISLib, using 100 estimators. K-fold fitting with five splits and ten repeats were used to parameterize the model. The input training data was split into an 80:20 ratio for modeling and testing. As the study site intersects four UTM zones, the output bathymetric models were combined and mosaicked onto a common grid. To create this, a WGS84 5 $\times$ 5 vector grid of 1° cells was generated and RSGISLib tools were used to intersect a vector tile index of the bathymetry models within it. For each vector grid cell, each image that intersected it was resampled with a nearest neighbor interpolation to that grid. The bathymetry models were then reduced to a single image using four descriptive statistics; mean, median, max and standard deviation. This resulted in 25 individual composite bathymetry images per statistic (e.g., max), derived from each bathymetry model that intersected a given grid cell. The 25 grid cells, now all on a common reference frame, were mosaicked to create one image. The benefit of this was that the reduction is done on a per-pixel basis per grid cell and this circumvented image edge effects common with tiling multiple acquisitions.

E. Validation

The bathymetric photons were not validated as they were generated at a much higher spatial resolution and vertical accuracy than existing bathymetric models, particularly those derived over large regional areas, as shown in [25]. For this reason, independent ICESat-2 data was used in the Landsat-derived bathymetry model validation. From the 95% remaining bathymetric photons data bank (see Section II-B), we excluded the extreme shallow water values outside of Andros Island leaving 15 583 933 points for validation. The maximum, median and mean pixel values from the bathymetry models were extracted for each validation bathymetry point. The root mean square error (RMSE) was then calculated from the residual error for each model.

III. Results

A. ICESat-2 Bathymteric Extraction

Bathymetric photons were successfully extracted from the ICESat-2 tracks, where a subaquatic surface was detected. The extraction model was able to run automatically with the user required only to select the threshold value that yielded the highest signal-to-noise ratio. An example of the extracted photons is visible in Fig. 3. A total of approximately 19 million individual bathymetric depths were detected, providing results at a much more time and economically efficient rate than field-based surveys. The extracted photons covered an area from 21.611955° to 27.636068° latitude and −79.470479° to −74.752996° longitude. The minimum depth values extracted were 0.75 m and the maximum depths were 30.45 m, with a mean and median depth of 4.69 and 4.26 m, respectively. The reduced training data size of 947 748 (5%) depth locations had a minimum depth of 0.75 m and a maximum depth of 30.3 m (median 4.3 m). The subsequently withheld validation data contained corresponding minimum and maximum depths of 0.75 and 30.45 m, respectively. The model was robust against false positives which could be readily excluded with the user-defined density threshold. The model was successful over a wide turbidity gradient, interpreted by the density of noise photons, successfully extracting surfaces in both clear and turbid conditions. At greater depths of $\geq$40 m, there was a low density of subaquatic returns and thus these depths could not be extracted. Where there was a strong return from a subaquatic depth, this was not a limitation.

B. Landsat Derived Bathymetry Models

A total of 221 individual bathymetry models were created and were successfully reduced into three spatially continuous

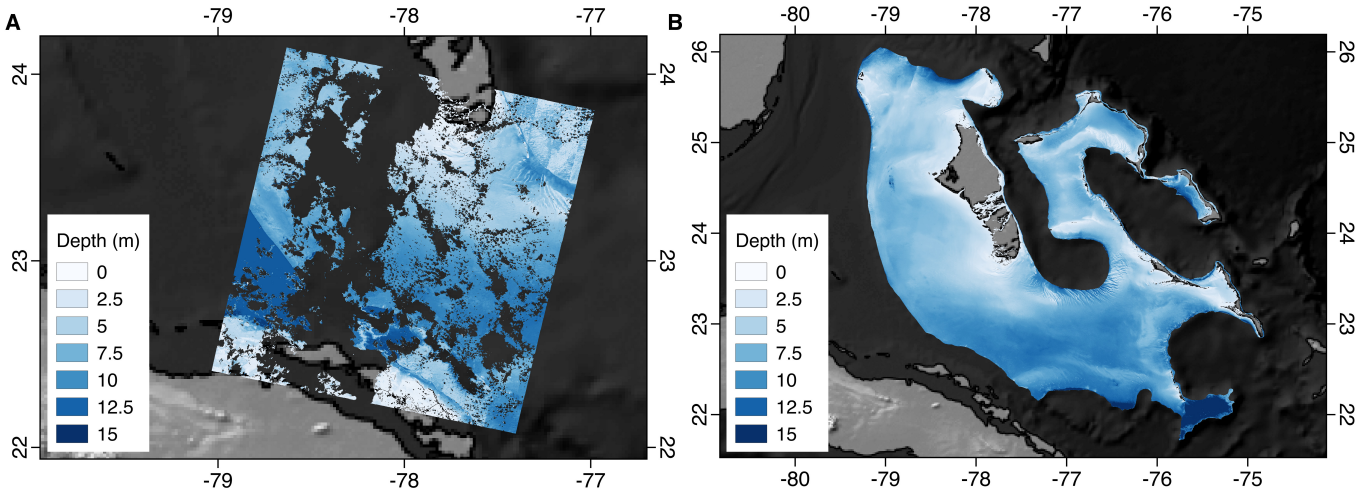

Fig. 4. Single bathymetric model generated from a single Landsat image (Left) and a spatially continuous median composite for the Bahamas region (Right) demonstrating a range of depths, with the deepest depths at the outer edge of the island complexes, such as at the Tongue of the Ocean.

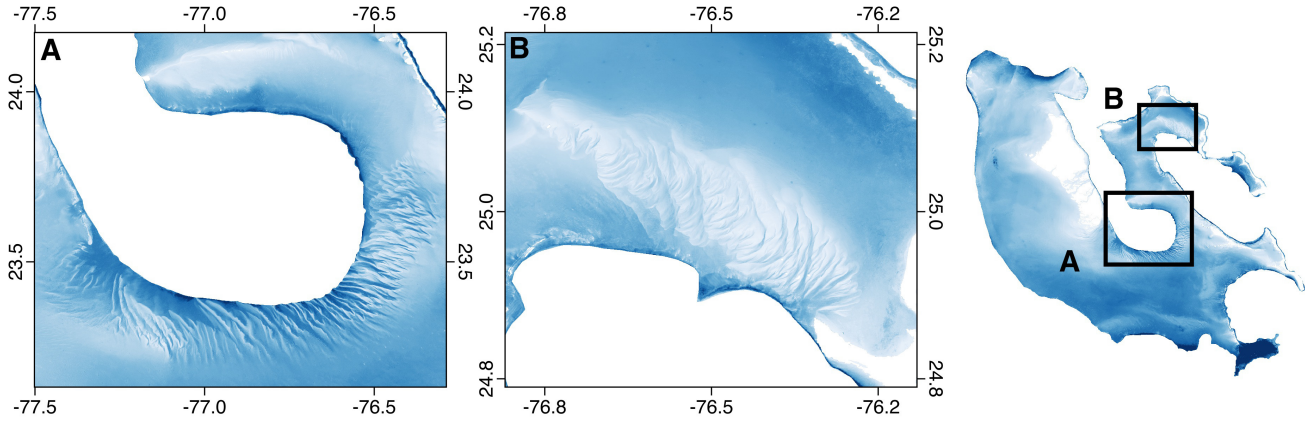

Fig. 5. Geomorphological features mapped with the bathymetry model. (a) and (b) Two distinct features with fine-scale variations in elevation.

models, representing the median, max, and mean depths for the study site. The median model is provided in Fig. 4.

The median and mean composites are visually comparable, with the models closely following the patterns observed in high-resolution imagery (e.g., Google Earth/MAXAR). Shallowest waters are observed around the island of Andros and shoal complexes around Schooner Cay, Exuma Cay, and the Great Bahamas Bank (Fig. 5) are observed, with water depth increasing toward the outer edges of the bay. Both maps contained a noisy speckled region, indicative of error in the model and not accurate derivation of depth. The maximum depth contained broadly similar patterns but had increased noise from the selection of the maximum pixel depth selection and some image edge effects were visible. The maximum composite produced the lowest quality esthetic product.

C. Validation

Overall the median composite had the lowest RMSE from 15 583 933 independent validation points in the Andros shallow water region. The median composite produced the lowest RMSE of 0.32 m, closely followed by the mean bathymetry composite of 0.35 m. The maximum composite had a substantially larger RMSE of 1.25 m. Each Landsat derived bathymetry model was accompanied by its own model performance metrics, using the internal training:testing split on an 80:20 ratio and estimates of residual error and its distribution. Also provided are the k–fold cross-validations to reflect the robustness of each Extra Trees Regressor (Table I). For the median composite, we assessed the change in absolute residual error with depth, with the majority of errors rarely exceeding 20 cm and occurring predominantly at shallower depths. Absolute error did not increase with model depth. This is shown in Fig. 6 alongside validation summary statistics of the three composites.

As the bathymetry models are composed of composite values from a range of individual models, it was possible to calculate per-pixel standard deviation and standard error (Fig. 7). Both standard deviation and standard error were low, ≤ 0.5 and ≤ 1.25, respectively, across the majority of the study site and larger values occurring at deeper bathymetric depth estimates. This figure also highlights a region of deep

TABLE I
5 OF 50 K-FOLD MODEL RESULTS FOR A SINGLE LANDSAT DERIVED BATHYMETRY MODEL

n	r2	explained variance score	median absolute error (m)	mean absolute error (m)	mean squared error (m)	root mean squared error (m)	norm root squared mean error (m)	bias (m)	norm bias (m)	bias squared (m)	variance (m)	noise (m)
0	0.970	0.970	0.141	0.235	0.164	0.404	8.042	-0.001	-0.022	0.000	0.164	0.000
1	0.968	0.968	0.142	0.236	0.175	0.418	8.325	-0.010	-0.194	0.000	0.175	0.000
2	0.969	0.969	0.144	0.239	0.171	0.414	8.217	-0.003	-0.063	0.000	0.171	0.000
3	0.969	0.969	0.143	0.237	0.175	0.419	8.343	-0.011	-0.220	0.000	0.175	0.000
4	0.971	0.971	0.142	0.235	0.160	0.400	7.947	-0.006	-0.123	0.000	0.160	0.000
5	0.968	0.968	0.142	0.238	0.178	0.422	8.359	-0.010	-0.192	0.000	0.178	0.000

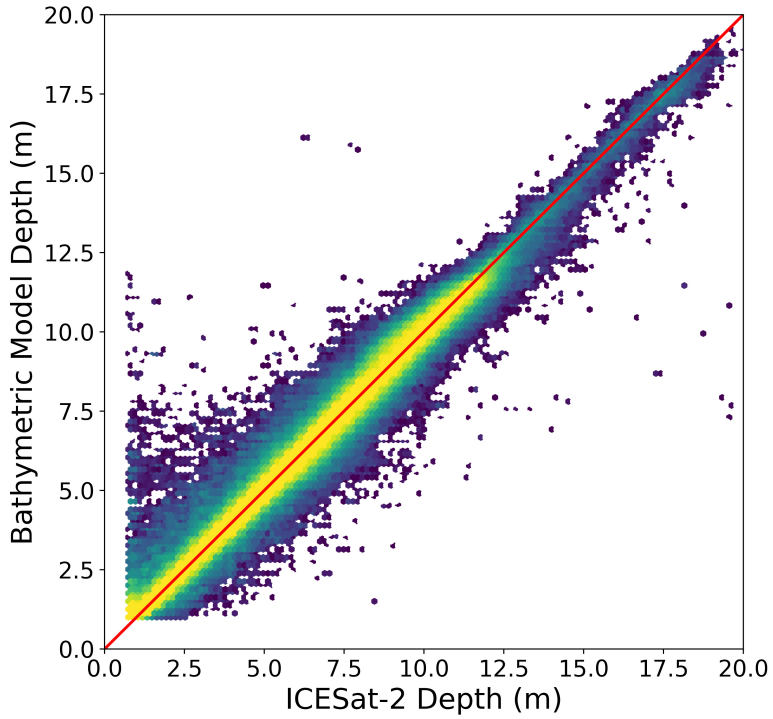

	RMSE	RMSE%	R^2
Max	1.25	22.1	0.89
Med	0.33	6.7	0.99
Mean	0.35	7.1	0.99

Fig. 6. (Left) Relationship between ICESat–2 observed depth and modeled depth. There is no relationship between depth and residual error, with the majority of errors being small and occurring across all depths. (Right) Summary statistics of the validation data for each of the three composite bathymetry maps.

bathymetry within the shallow bay (24.5° N, −79.3° E), interpreted as model noise and not accurate derivation of depth.

IV. DISCUSSION

We have developed an open source workflow for regional-scale bathymetry mapping from purely spaceborne data, capable of generating maps with low error. We demonstrate C-SHELPh, a means of automating the extraction of bathymetric photons from ICESat-2 tracks, capable of the required orthometric calibration and geometric correction of the photons caused by the refraction of the laser at the air/ocean interface. C-SHELPh was able to extract photons to depths of 40 m, making it suitable for nearshore coastal waters. The extraction of 224 ICESat-2 tracks totaling 18 954 960 points demonstrates the ability of C-SHELPh to work at scale to create large training banks of data for regional-scale studies. Further developments to C-SHELPh could include the extraction of a detailed water surface to characterize waves and the automated online lookup of water salinity, to further the accuracy of the refraction correction. The simplistic approach of C-SHELPh to detect point density over a grid enables it to be readily tuned and modified, allowing it to be specifically customized. In some instances, in very shallow ($\leq$0.5 m) waters C-SHELPh is susceptible to the under-classification of bathymetric photons as the sea surface is approached and confusion increases. This parameter is, however, customizable within the algorithm and this confusion can be mitigated against. This approach is more standardized and simplistic than [32] and achieves satisfactory results. Furthermore, as C-SHELPh is written in python it can fit easily into existing open source workflows and is open to the community for modification and improvement.

Our use of a machine learning regressor was able to generate regional-scale spatially continuous seamless composites of bathymetry, with high model accuracy and low RMSE values of 0.32 m. We were able to utilize a state-of-the-art algorithm in a field that has traditionally relied on linear relationships [17], [18] between variables, allowing us to exploit both linear and nonlinear relationships to derive improved results.

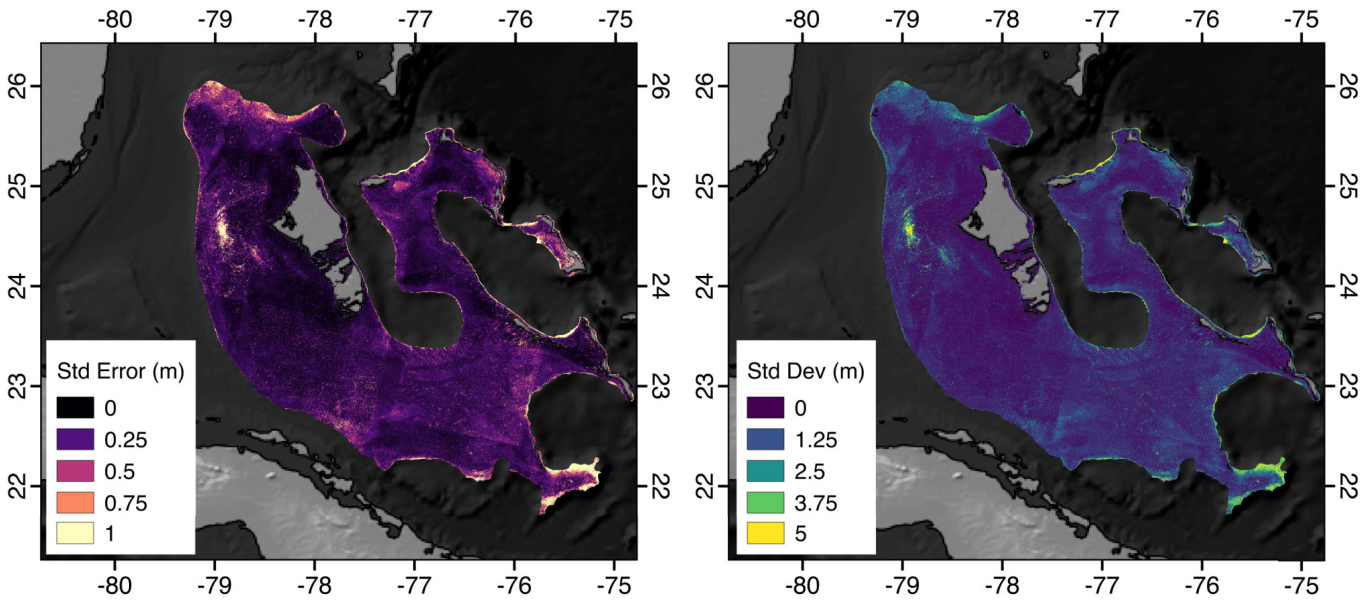

Fig. 7. (Left) Standard error map of the region, detailing increased errors at increased depths. (Right) Standard deviation map of the study site used to determine standard error. A region of inaccurately modeled deep bathymetry within the shallow bay at 24.5° N, −79.3° E, is visible.

Traditionally, nonlinearity in models increases uncertainties, but a machine learning algorithm is able to exploit this to reduce overall error. These models were capable of using millions of data points for robust modeling and validation while remaining vigorous against overfitting. Our workflow is built upon RSGISLib [42] to enable efficient access to advanced scikit-learn [43] machine learning algorithms and model parametrization. Tools within RSGISLib allow the efficient extraction of raster–to–point values for training and validation, efficient regridding of the results to a common frame and the reduction of over 200 bathymetry images to a single seamless mosaic, easily formed into a workflow through python bindings and enabling the integration of other common python modules such as Pandas, GeoPandas and Matplotlib. This efficiency enabled a regional-scale bathymetry map to be created at high spatial resolution (30 m), allowing high spatial detail to be mapped, such as geomorphological features. The ability to process hundreds of individual Landsat scenes reduces the reliance upon image composites which have been used in cloudy regions to date, sometimes spanning numerous years [25]. This reduces image artifacts, such as cloud edges and image edge–effects, which are known to degrade optical composites, while combining pixels with varying reflectance values due to atmospheric conditions and solar angle. Instead, compositing the bathymetry models enables several maps to be generated at once, including minimum, maximum, mean and median, rather than just one single model. However, the model is not limited to this limited number of statistical descriptors, in fact, any statistical reduction can be used to determine the most accurate model. This allows full flexibility in the workflow to generate the most robust bathymetric model. Furthermore, the use of individual images enables the derivation of per–pixel variance and maps of bathymetry standard deviation and standard error. This enables the spatial distribution of uncertainty to be mapped across the study site at high resolution. Per–image model statistics are also generated for detailed assessment of each model, including internal residual scores and model fit. Finally, this workflow is not limited to Landsat data alone and is applicable to any visible wavelength imagery, thus it can be applied to Sentinel-2, PlanetScope and MAXAR data to derive increased spatial resolution if required.

The acquisition of bathymetry maps from purely spaceborne data is being more readily facilitated, yet standardized methods are still in their infancy and machine learning algorithms have yet to be fully explored, with numerous studies utilizing traditional linear methods [25], [33], [35], [44], [45]. We demonstrate that machine learning algorithms are well placed to tackle nonlinear relationships between reflectance and ocean depth, evidenced by the low uncertainties measured in this study. Future work could focus on the use of additional machine learning algorithms and further exploration of model parametrization, including the use of additional optical bands, such as the Landsat coastal band, as well as associated band ratio combinations and statistical reducers (e.g., mode, percentiles) in addition to the of maximum, mean and median. Furthermore, our approach is applicable to all optical remote sensing imagery with short wavelength visible bands, thus from an applications perspective, the use of additional data such as Sentinel-2 and PlanetScope/MAXAR imagery should be investigated.

V. Conclusion

We provide a means of end-to-end bathymetry mapping with purely spaceborne data. We map the shallow waters around the Bahamas island of Andros, extracting 224 separate ICESat-2 bathymetric photon tracks and fusing them with 221 Landsat 8 images to create a single bathymetric map with an RMSE

of 0.33 m. Our open source workflow, based upon mature and efficient software and advanced machine learning algorithms, paves the way for anyone to have access to contemporary regional-scale bathymetry mapping. Our open source approach will enable the community to further the mapping and ecosystem accounting of important blue carbon coastal environments by providing more readily accessible spatially continuous maps of ocean depth and subaquatic structure. The ability to derive spaceborne bathymetric models will help advance studies into habitat characterization, storm surge modeling, coastal protection, fisheries, and sea level rise as well as other sciences that serve the Blue Economy.

ACKNOWLEDGMENT

The authors would like to thank members of the ICESat-2 Science Team Bathymetry Working Group for their feedback during algorithm/workflow development. The authors would also like to acknowledge all of the open source software that made the workflow presented possible.

CODE AVAILABILITY

All code is available in the C-SHELPh GitHub repository: https://zenodo.org/record/6282224#.Yhj2Oi-B2yE

REFERENCES

[1] A. LiVecchi *et al.*, "Powering the blue economy; exploring opportunities for marine renewable energy in maritime markets," U.S. Dept. Energy, Office Energy Efficiency Renew. Energy, Washington, DC, USA, Tech. Rep., 2019, p. 207.

[2] M. M. Foley *et al.*, "Guiding ecological principles for marine spatial planning," *Mar. Policy*, vol. 34, no. 5, pp. 955–966, Sep. 2010.

[3] S. E. Lester, C. White, K. Mayall, and R. K. Walter, "Environmental and economic implications of alternative cruise ship pathways in bermuda," *Ocean Coastal Manage.*, vol. 132, pp. 70–79, Nov. 2016.

[4] J. Flower *et al.*, "Marine spatial planning on the Caribbean island of montserrat: Lessons for data-limited small islands," *Conservation Sci. Pract.*, vol. 2, no. 4, p. e158, Apr. 2020.

[5] M. D. Spalding *et al.*, "The role of ecosystems in coastal protection: Adapting to climate change and coastal hazards," *Ocean Coastal Manage.*, vol. 90, pp. 50–57, Mar. 2014.

[6] S. Narayan *et al.*, "The effectiveness, costs and coastal protection benefits of natural and nature-based defences," *PLoS ONE*, vol. 11, no. 5, May 2016, Art. no. e0154735.

[7] M. J. A. Christianen *et al.*, "Low-canopy seagrass beds still provide important coastal protection services," *PLoS ONE*, vol. 8, no. 5, May 2013, Art. no. e62413.

[8] D. L. Harris *et al.*, "Coral reef structural complexity provides important coastal protection from waves under rising sea levels," *Sci. Adv.*, vol. 4, no. 2, Feb. 2018, Art. no. eaao4350.

[9] A.-C. Wölfl *et al.*, "Seafloor mapping—The challenge of a truly global ocean bathymetry," *Frontiers Mar. Sci.*, vol. 6, p. 283, Jun. 2019.

[10] K. Marks, "The IHO-IOC GEBCO cook book," Tech. Rep., 2019.

[11] S. Thierry, S. Dick, S. George, L. Benoit, and P. Cyrille, "EMODnet bathymetry a compilation of bathymetric data in the European waters," in *Proc. OCEANS*, Jun. 2019, pp. 1–7.

[12] D. C. Kapoor, "General bathymetric chart of the oceans (GEBCO)," *Mar. Geodesy*, vol. 5, no. 1, pp. 73–80, Jan. 1981.

[13] L. Janowski, K. Trzcinska, J. Tegowski, A. Kruss, M. Rucinska-Zjadacz, and P. Pocwiardowski, "Nearshore benthic habitat mapping based on multi-frequency, multibeam echosounder data using a combined object-based approach: A case study from the Rowy site in the southern Baltic sea," *Remote Sens.*, vol. 10, no. 12, p. 1983, Dec. 2018.

[14] H. Kim, S. B. Lee, and K. S. Min, "Shoreline change analysis using airborne LiDAR bathymetry for coastal monitoring," *J. Coastal Res.*, vol. 79, pp. 269–273, Mar. 2017.

[15] I. Caballero, R. P. Stumpf, and A. Meredith, "Preliminary assessment of turbidity and chlorophyll impact on bathymetry derived from Sentinel-2A and Sentinel-3A satellites in South Florida," *Remote Sens.*, vol. 11, no. 6, p. 645, Mar. 2019.

[16] I. Caballero and R. Stumpf, "Atmospheric correction for satellite-derived bathymetry in the Caribbean waters: From a single image to multi-temporal approaches using Sentinel-2A / B," *Opt. Exp.*, vol. 28, no. 8, pp. 11742–11766, 2020.

[17] D. R. Lyzenga, N. P. Malinas, and F. J. Tanis, "Multispectral bathymetry using a simple physically based algorithm," *IEEE Trans. Geosci. Remote Sens.*, vol. 44, no. 8, pp. 2251–2259, Aug. 2006.

[18] R. P. Stumpf, K. Holderied, and M. Sinclair, "Determination of water depth with high-resolution satellite imagery over variable bottom types," *Limnol. Oceanogr.*, vol. 48, pp. 547–556, Jan. 2003.

[19] G. Casal, P. Harris, X. Monteys, J. Hedley, C. Cahalane, and T. McCarthy, "Understanding satellite-derived bathymetry using Sentinel 2 imagery and spatial prediction models," *GISci. Remote Sens.*, vol. 57, no. 3, pp. 271–286, Apr. 2020.

[20] J. Li *et al.*, "Adaptive bathymetry estimation for shallow coastal waters using planet dove satellites," *Remote Sens. Environ.*, vol. 232, Oct. 2019, Art. no. 111302.

[21] M. B. Lyons *et al.*, "Mapping the world's coral reefs using a global multiscale Earth observation framework," *Remote Sens. Ecol. Conservation*, vol. 6, no. 4, pp. 557–568, Dec. 2020.

[22] V. Mateo-Pérez, M. Corral-Bobadilla, F. Ortega-Fernández, and E. P. Vergara-González, "Port bathymetry mapping using support vector machine technique and Sentinel-2 satellite imagery," *Remote Sens.*, vol. 12, no. 13, p. 2069, Jun. 2020.

[23] D. Poursanidis, D. Traganos, P. Reinartz, and N. Chrysoulakis, "On the use of Sentinel-2 for coastal habitat mapping and satellite-derived bathymetry estimation using downscaled coastal aerosol band," *Int. J. Appl. Earth Observ. Geoinf.*, vol. 80, pp. 58–70, Aug. 2019.

[24] D. Traganos, D. Poursanidis, B. Aggarwal, N. Chrysoulakis, and P. Reinartz, "Estimating satellite-derived bathymetry (SDB) with the Google earth engine and Sentinel-2," *Remote Sens.*, vol. 10, no. 6, p. 859, Jun. 2018.

[25] N. Thomas *et al.*, "Space-borne cloud-native satellite-derived bathymetry (SDB) models using ICESat-2 and Sentinel-2," *Geophys. Res. Lett.*, vol. 48, no. 6, Mar. 2021, Art. no. e2020GL092170.

[26] A. Le Quilleuc, A. Collin, M. F. Jasinski, and R. Devillers, "Very high-resolution satellite-derived bathymetry and habitat mapping using Pleiades-1 and ICESat-2," *Remote Sens.*, vol. 14, no. 1, p. 133, Dec. 2021.

[27] C. E. Parrish, L. A. Magruder, A. L. Neuenschwander, N. Forfinski-Sarkozi, M. Alonzo, and M. Jasinski, "Validation of ICESat-2 ATLAS bathymetry and analysis of ATLAS's bathymetric mapping performance," *Remote Sens.*, vol. 11, no. 14, p. 1634, Jul. 2019.

[28] Y. Chen, Z. Zhu, Y. Le, Z. Qiu, C. Gang, and L. Wang, "Refraction correction and coordinate displacement compensation in nearshore bathymetry using ICESat-2 LiDAR data and remote-sensing images," *Opt. Exp.*, vol. 29, no. 2, pp. 2411–2430, 2021.

[29] J. Halls and K. Costin, "Submerged and emergent land cover and bathymetric mapping of estuarine habitats using WorldView-2 and LiDAR imagery," *Remote Sens.*, vol. 8, no. 9, p. 718, Aug. 2016.

[30] R. Abileah, "Mapping near shore bathymetry using wave kinematics in a time series of WorldView-2 satellite images," in *Proc. IEEE Int. Geosci. Remote Sens. Symp. (IGARSS)*, Jul. 2013, pp. 2274–2277.

[31] T. Sagawa, Y. Yamashita, T. Okumura, and T. Yamanokuchi, "Satellite derived bathymetry using machine learning and multi-temporal satellite images," *Remote Sens.*, vol. 11, no. 10, p. 1155, May 2019.

[32] H. Ranndal, P. S. Christiansen, P. Kliving, O. B. Andersen, and K. Nielsen, "Evaluation of a statistical approach for extracting shallow water bathymetry signals from ICESat-2 ATL03 photon data," *Remote Sens.*, vol. 13, no. 17, p. 3548, Sep. 2021.

[33] B. J. Babbel, C. E. Parrish, and L. A. Magruder, "ICESat-2 elevation retrievals in support of satellite-derived bathymetry for global science applications," *Geophys. Res. Lett.*, vol. 48, no. 5, pp. 1–9, Mar. 2021.

[34] A. C. R. Gleason, R. Smith, S. J. Purkis, K. Goodrich, A. Dempsey, and A. Mantero, "The prospect of global coral reef bathymetry by combining ice, cloud, and land elevation Satellite-2 altimetry with multispectral satellite imagery," *Frontiers Mar. Sci.*, vol. 8, p. 1529, Oct. 2021.

[35] A. Albright and C. Glennie, "Nearshore bathymetry from fusion of Sentinel-2 and ICESat-2 observations," *IEEE Geosci. Remote Sens. Lett.*, vol. 18, no. 5, pp. 900–904, May 2021.

[36] Y. Ma *et al.*, "Satellite-derived bathymetry using the ICESat-2 LiDAR and Sentinel-2 imagery datasets," *Remote Sens. Environ.*, vol. 250, Dec. 2020, Art. no. 112047.
[37] T. A. Neumann *et al.*, "ATLAS/ICESat-2 L2A global geolocated photon data, version 3," NASA Nat. Snow Ice Data Center Distrib. Active Archive Center, Boulder, CO, USA, Tech. Rep., 2020, vol. 10.
[38] T. Markus *et al.*, "The ice, cloud, and land elevation satellite-2 (ICESat-2): Science requirements, concept, and implementation," *Remote Sens. Environ.*, vol. 190, pp. 260–273, Mar. 2017.
[39] J. Scheick *et al.* (2019). *IcePyx: Python Tools for Obtaining and Working With ICESat-2 Data*. ICESat-2py. [Online]. Available: https://github.com/icesat2py/icepyx
[40] R. W. Reynolds, T. M. Smith, C. Liu, D. B. Chelton, K. S. Casey, and M. G. Schlax, "Daily high-resolution-blended analyses for sea surface temperature," *J. Climate*, vol. 20, pp. 5473–5496, Nov. 2007.
[41] P. Bunting *et al.*, "The global mangrove watch—A new 2010 global baseline of mangrove extent," *Remote Sens.*, vol. 10, no. 10, p. 1669, Oct. 2018.
[42] P. Bunting, D. Clewley, R. M. Lucas, and S. Gillingham, "The remote sensing and GIS software library (RSGISLib)," *Comput. Geosci.*, vol. 62, pp. 216–226, Jan. 2014, doi: 10.1016/j.cageo.2013.08.007.
[43] F. Pedregosa *et al.*, "Scikit-learn: Machine learning in Python," *J. Mach. Learn. Res.*, vol. 12 no. 10, pp. 2825–2830, 2011.
[44] D. Traganos, B. Aggarwal, D. Poursanidis, K. Topouzelis, N. Chrysoulakis, and P. Reinartz, "Towards global-scale seagrass mapping and monitoring using Sentinel-2 on Google Earth engine: The case study of the Aegean and ionian seas," *Remote Sens.*, vol. 10, no. 8, p. 1227, Aug. 2018.
[45] D. Poursanidis, D. Traganos, N. Chrysoulakis, and P. Reinartz, "Cubesats allow high spatiotemporal estimates of satellite-derived bathymetry," *Remote Sens.*, vol. 11, no. 11, p. 1299, May 2019.

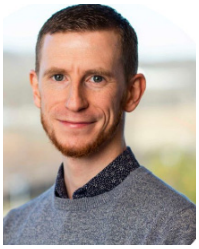

Nathan Thomas is a University of Maryland (UMD) Earth System Science Interdisciplinary Center (ESSIC) Assistant Research Scientist with the NASA Goddard Space Flight Center, Greenbelt, MD, USA. His research revolves around the use of both active and passive systems for mapping blue carbon ecosystems and their structure.

Brian Lee is pursuing the Ph.D. degree with the Bren School of Environmental Science, University of California, Santa Barbara, CA, USA.

His research focuses on leveraging active remote sensing datasets to study interactions between natural and human-dominated systems.

Oliver Coutts pursuing the master's degree in earth observation from Aberystwyth University, Wales, U.K., where he wrote his thesis on data fusion between Landsat and ICESat-2 data for estimating bathymetric depths in coastal waters.

Pete Bunting is a Reader in remote sensing with Aberystwyth University, Wales, U.K. His research is focused on the use of remote sensing data for environmental applications. Currently, he has a particular focus on the Global Mangrove Watch. He also maintains the RSGISLib software.

David Lagomasino is an Assistant Professor in the interdisciplinary integrated coastal programs with East Carolina University, Wanchese, NC, USA. He studies how natural and human-related changes impact the function of coastal ecosystems using various remote sensing instruments. He serves on several blue carbon and coastal ecosystem advisory committees.

Lola Fatoyinbo is a Research Physical Scientist with the Biospheric Sciences Laboratory, NASA Goddard Space Flight Center, Greenbelt, MD, USA, where she studies forest ecology and ecosystem structure using active and passive remote sensing instruments, serves on Satellite Mission Science Teams and is Principal Investigator on several NASA Earth Science Division funded research grants.